Inorganic Chemistry

Communication

pubs.acs.org/IC

Formation of Self-Assembled Defect-Free Zn_2SnO_4 Nanostructures from Binary Oxides without the Kirkendall Effect

Partha Pratim Das[†,‡] and Parukuttyamma Sujatha Devi*[,†,‡]

[†]Nano-Structured Materials Division, Council of Scientific & Industrial Research (CSIR)—Central Glass and Ceramic Research Institute, Kolkata 700032, India

[‡]CSIR-Network Institute of Solar Energy, New Delhi India

Supporting Information

ABSTRACT: In this Communication, we report a facile approach to synthesize a technologically important oxide Zn_2SnO_4 (ZTO) by a temperature-dependent solid-state reaction without the Kirkendall effect. Single-phase defect-free ZTO was formed upon calcination of a homogeneous 2:1 mixture of reactive ZnO rods and SnO_2 nanoparticles at 1000 °C. We also observed interesting photocatalytic and photovoltaic properties from the synthesized ZTO material.

The ternary complex oxide zinc stannate, Zn_2SnO_4 (ZTO), is an important n-type semiconducting oxide with a typical inverse 2−4 cubic spinel structure with the *Fd*3*m* space group. This mixed oxide exhibits high electron mobility (10−15 $cm^2 V^{-1} s^{-1}$), high electrical conductivity, adequate thermodynamic stability, and low visible absorption with a band gap of 3.6 eV.[1] Interestingly, the compound ZTO also exhibits better properties than its binary counterparts ZnO and SnO_2, and therefore ZTO is a potential candidate for dye-sensitized solar cells (DSSCs),[2] and photocatalysis.[3] In addition, other minor applications such as, sensors, transparent conducting electrodes, and electrodes for lithium batteries are also being explored. Because of its complex nature, the synthesis of phase-pure ZTO has been a highly challenging task. The ZTO nanostructures have mainly been synthesized by hydrothermal reaction.[2a,d,3a,b,4] In addition, there are also scattered reports on chemical vapor deposition, thermal evaporation, mechanical grinding, high-temperature calcination, and sol−gel technique for the synthesis of ZTO.[5] In many cases, the synthesized ZTO also lacks phase purity and exhibits the presence of impure phases like ZnO or SnO_2. Therefore, considering the potential application of ZTO in photovoltaic and photocatalytic applications, we have designed a cost-effective facile approach, yielding a high percentage of defect-free and impurity-free ZTO.

Here, we report the one-step synthesis of defect-free cubic spinel ZTO by calcining a 2:1 mixture of hexagonal ZnO rods and tetragonal SnO_2 nanoparticles at 1000 °C. The starting materials, ZnO rods and SnO_2 nanoparticles, were synthesized through a solution-processed sonochemical technique, followed by thermal annealing at 300 and 600 °C, respectively.[6] For a typical batch synthesis of ZTO, ZnO rods and SnO_2 particles were mixed in a molar ratio of 2:1 and ground thoroughly in an agate mortar using ethanol to make it homogeneous (Supporting Information, SI). Thermogravimetric (TG) investigation of the mixture indicated only a very small weight loss of 0.42% up to 1200 °C. The presence of a small exothermic peak around 878 °C in the differential scanning calorimetric (DSC) data, on the other hand, confirms the crystallization of ZTO (Figure S1 in the SI). Thus, on the basis of thermal studies, the well-ground mixture was calcined at 1000 °C for 8 h. To explore the temperature-dependent evolution of the ZTO phase from a mixture of ZnO and SnO_2, we have carried out X-ray diffraction (XRD) analysis of the starting materials and intermediate products. The comparative XRD patterns of ZnO rods, SnO_2 particles, the mixture, and the calcined products are presented in Figure 1. The XRD

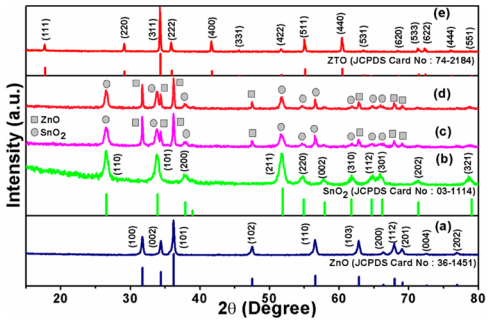

Figure 1. XRD patterns of (a) ZnO, (b) SnO_2, (c) the 2:1 ratio of ZnO and SnO_2, and the mixture calcined at (d) 800 and (e) 1000 °C.

reflections of the precursors ZnO (Figure 1a) and SnO_2 (Figure 1b) exactly match with the hexagonal ZnO (JCPDS 36-1451) and tetragonal SnO_2 (JCPDS 03-1114), respectively, as shown in the figure. The calculated lattice parameters of the employed ZnO were a = 3.252 Å and c = 5.208 Å, whereas those of SnO_2 were a = 4.736 Å and c = 3.183 Å. The mixture calcined at 800 °C (Figure 1d) also exhibited reflections corresponding to the ZnO and SnO_2 phases similar to the starting mixture (Figure 1c). This indicates the absence of any reaction occurring between ZnO and SnO_2 up to 800 °C. The 1000 °C calcined mixture (Figure 1e), on the other hand, exhibited a different X-ray pattern, which appeared to be similar to the reported diffraction pattern of the cubic ZTO spinel phase (JCPDS 74-2184). The calculated lattice parameter of the formed ZTO was a = 8.717 Å, which is comparable to the reported lattice constant a = 8.650 Å of the cubic ZTO. From the XRD pattern, the successful formation of

Received: July 4, 2014
Published: October 6, 2014

the cubic spinel ZTO from a homogeneous mixture of hexagonal ZnO and tetragonal SnO_2 at 1000 °C has been confirmed. The reaction of 2ZnO + SnO_2 to form ZTO could occur as a result of a temperature-mediated diffusion-controlled solid-state reaction (SSR). Such interdiffusion reactions usually result in the formation of a porous layer on the more rapidly diffusing component between the interface of two materials, like ZnO and SnO_2 in this case.[7a−d] Therefore, in order to monitor the size and morphology of the final product formed and thereby understand the reaction mechanism, extensive morphological characterizations were carried. The representative microscopic images are presented in Figures 2a−d and S2, S3 in the SI. It is evident from

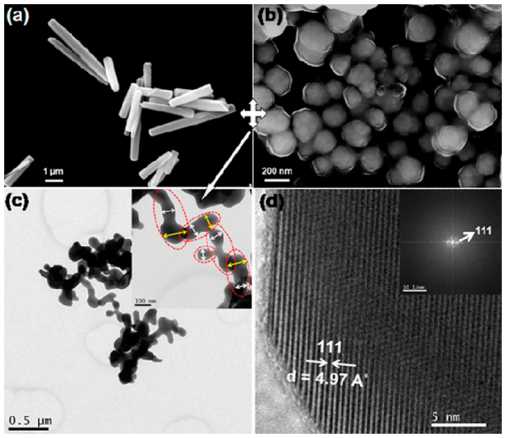

Figure 2. (a) SEM image of ZnO rods, FESEM image of (b) SnO_2 nanoparticles, (c) TEM image of the mixture calcined at 1000 °C, along with the image at high magnification (inset), and (d) HRTEM image of the calcined mixture, along with the FFT of the particular HRTEM (inset).

the SEM, FESEM, and TEM images that the rod shape of the precursor ZnO having length between 1 and 5 μm and a diameter of ∼350 nm (Figures 2a and S2a in the SI) and the spherical morphology of SnO_2 nanoparticles of sizes of around 10−20 nm (Figures 2b and S2d in the SI). The high-resolution (HR)TEM images confirm the single-crystalline nature of the individual ZnO rods and SnO_2 nanoparticles, where the spacing corresponds to the (002) and (110) reflections of ZnO and SnO_2, respectively (Figure S2b,e in the SI). The FESEM image of the 2:1 mixture (Figure S3a in the SI) after grinding shows the attachment of SnO_2 nanoparticles onto the ZnO rod surface without sacrificing their individual morphology and size. After calcination, on the other hand, significant changes in the morphology and size of the starting materials were noticed. The final product exhibited neither rod nor particle shape, as is evident from the microstructures (Figure 2c). Interestingly, with the concomitant formation of ZTO, the formation of elongated but dense particles without any Kirkendall pore formation was noticed. The formed elongated particles exhibited widths of 50−100 nm and a length of 300 nm, as is evident from the marked TEM image shown in the inset of Figure 2c. It appears as if the initially attached SnO_2 particles have diffused into the rod-shaped ZnO during calcination, and subsequent SSR resulted in the formation of elongated dense ZTO particles, which are attached to one another like a self-assembled chain, as is evident in the inset of Figure 2d. The SAED pattern shown in Figure S3b in the SI, further confirms the highly crystalline nature of the formed ZTO. It is interesting to note the formation of dense particles without any pores, confirming the absence of any preferential precipitation of ZTO on any of the binary oxide surfaces. The preferential precipitation of ZTO could also lead to the formation of disordered ZTO with nonequillibrium cation distribution.[5b] This evidence confirms a simple SSR between ZnO and SnO_2, leading to the formation of dense ZTO nanostructures without any Kirkendall effect.[7a−c] This has been attributed to the effect of the highly reactive starting materials that we have used. The above observation is in contrast to the report of Shi and Dai on the formation of porous ZTO tubes from ZnO nanorods through the Kirkendall effect.[3a] The HRTEM image confirms the single-crystalline lattice fringe measured as 4.97 Å corresponding to the (111) reflection of cubic ZTO. It is interesting to monitor the change in the morphology of the starting materials from rods and particles to elongated assembled particles during the formation of ZTO.

The room temperature UV−vis absorption and diffuse-reflectance spectrum of the prepared ZTO are shown in Figure S4 in the SI. The steep absorption spectrum that started to ascend around 350 nm is ascribed to the intrinsic band-gap transition of ZTO. Extrapolation of the linear part of the absorption edge corresponds to the band gap (E_g) of 3.8 eV, which is quite analogous to the reported band gaps in the range of 3.2−3.9 eV for ZTO.[3a] In order to further assess the structural quality of the phase formed, Raman spectra have been measured with a 514 nm Ar^+ laser line at room temperature. In Figure 3, the Raman spectra

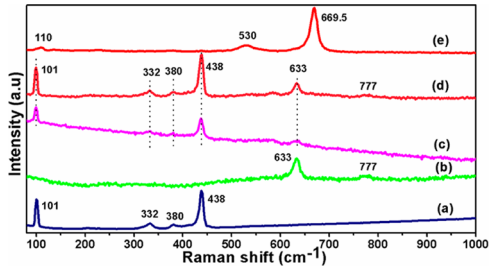

Figure 3. Raman spectra of (a) ZnO, (b) SnO_2, (c) a ZnO and SnO_2 mixture, and a mixture calcined at (d) 800 and (e) 1000 °C, respectively.

of ZnO rods, SnO_2 particles, the mixture, and the mixture calcined at 800 and 1000 °C, respectively, are presented. The prime peak at 438 cm^{-1} for the precursor ZnO is attributed to the Raman-active E_2 mode characteristic of the hexagonal wurtzite phase. The observed additional bands at 101 and 380 cm^{-1} are assigned to the E_2^{low} and A_1 (LO) modes, whereas the band at 332 cm^{-1} is due to the multiphonon scattering process (Figure 3a). The precursor SnO_2 exhibited characteristic Raman scattering peaks at 633 and 777 cm^{-1}, which respectively correspond to the A_{1g} and B_{2g} vibration modes of the tetragonal SnO_2 (Figure 3b).

As expected, the ground mixture of 2ZnO + SnO_2 exhibited the Raman-active modes of both ZnO and SnO_2 (Figure 3c). It is worth noting the retention of the above Raman bands up to the calcination temperature of 800 °C, confirming the presence of only unreacted oxides up to this temperature, which corroborates the XRD results shown in Figure 1d. Finally, upon calcination at 1000 °C, an intense Raman-active band appeared at 669.5 cm^{-1} corresponding to the A_{1g} symmetric vibration of the Zn−O bonds in the ZnO_4 tetrahedra of a fully inverse ZTO spinel.[5b] Another phonon mode at 530 cm^{-1} corresponds to the F_{2g} symmetric bending of oxygen atoms in the M−O bonds of the MO_6 octahedra (M = Zn or Sn). The most interesting observation is the absence of a Raman band at 626 cm^{-1}, which unambiguously confirms the formation of defect-free cubic spinel ZTO by this

dx.doi.org/10.1021/ic501598h | Inorg. Chem. 2014, 53, 10797−10799

process (Figure 3e).[5b] This further corroborates our conformation of the formation of phase-pure dense ZTO nanostructures by a SSR without any Kirkendall effect. In order to evaluate the quality of the synthesized ZTO nanostructures, we have also carried out some preliminary experiments on the photocatalytic activity and DSSC efficiency of the same. The photocatalytic activity of the as-prepared ZTO was investigated using the textile dye Methylene Blue (MB), which is a major contaminant in the wastewater.

The time-dependent absorption spectra of a MB solution upon exposure to UV light, shown in Figure 4, exhibited a gradual

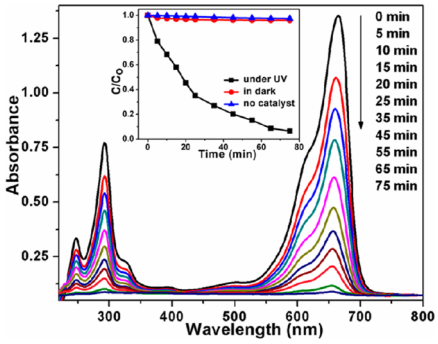

Figure 4. UV−vis absorption spectra of a MB solution in the presence of ZTO under UV light at different time intervals. Inset: C/C_0 of MB versus time at different conditions.

decrease in the absorbance bands centered at 665 and 292 nm, which disappeared completely after 75 min, suggesting the high photocatalytic activity of the prepared material. The inset shows changes in the concentration of MB with time, where C_0 and C respectively signify the concentrations of MB before and after UV exposure. Only a negligible change in the concentration of MB was noticed in the dark. Interestingly, a similar trend was observed in the absence of the catalyst. The observed color change indicated the removal of MB in the solution because of its photocatalytic degradation in the presence of ZTO, which acted as an efficient photocatalyst. The loss in activity of the catalyst was negligible after repeated usage, suggesting a higher stability of ZTO as a photocatalyst. In addition, we have also carried out some preliminary studies to use the prepared ZTO as a photoanode for DSSC application similar to the conditions used for ZnO rods.[6a] The preliminary studies with N719 dye molecule exhibited an extraordinarily high V_{oc} of 0.8605 ± 0.01 V and a fill factor of 73.76, although the measured efficiency was below 1%. The V_{oc} values reported for ZTO-based devices varied from 0.51 V to a maximum of 0.82 V.[2] The observed V_{oc} of the device fabricated using the synthesized ZTO is interestingly higher than the reported values.[2] Experiments with different dye loadings and molecules are underway to exploit the utilization of this single-step-synthesized ZTO as an efficient photoanode in DSSCs. In summary, our results confirm that it is possible to synthesize defect-free, impurity-free, cubic spinel ZTO by a facile approach by calcining a 2:1 homogeneous mixture of reactive hexagonal ZnO rods and tetragonal SnO_2 nanoparticles at 1000 °C. The microstructural investigations manifested a significant change in the morphology of the final product ZTO compared to the binary oxides. This could be one of the simplest, versatile, and economically viable techniques investigated for the synthesis of this technologically potent oxide. Moreover, the ZTO prepared by this single-step process could be projected as an efficient photocatalyst for wastewater treatment.

■ ASSOCIATED CONTENT

Supporting Information

Experimental details, TG−DSC data, TEM and HRTEM images, corresponding FFT and SAED patterns of ZnO rods and SnO_2 nanoparticles, FESEM of the ground mixture of ZnO and SnO_2, SAED pattern of ZTO, and UV−vis and diffuse-reflectance data. This material is available free of charge via the Internet at http://pubs.acs.org.

■ AUTHOR INFORMATION

Corresponding Author

*E-mail: psujathadevi@cgcri.res.in or psujathadevi@gmail.com.

Notes

The authors declare no competing financial interest.

■ ACKNOWLEDGMENTS

P.S.D. acknowledges Ministry of New and Renewable Energy (MNRE) for financial support under the CSIR-TAPSUN program. P.P.D. acknowledges financial support from MNRE for fellowship. The authors also thank Dr. S. B. Ogale, Chief Scientist, CSIR-National Chemical Laboratory, Pune, India, for kindly providing the experimental facilities for DSSC cell testing.

■ REFERENCES

(1) (a) Coutts, T. J.; Young, D. L.; Li, X.; Mulligan, W. P.; Wu, X. *J. Vac. Sci. Technol. A* **2000**, *18*, 2646−2660. (b) Young, D. L.; Moutinho, H.; Yan, Y.; Coutts, T. J. *J. Appl. Phys.* **2002**, *92*, 310−319.

(2) (a) Tan, B.; Toman, E.; Li, Y.; Wu, Y. *J. Am. Chem. Soc.* **2007**, *129*, 4162−4163. (b) Miyauchi, M.; Liu, Z.; Zhao, Z.-G.; Anandan, S.; Hara, K. *Chem. Commun.* **2010**, *46*, 1529−1531. (c) Wang, Y. F.; Li, K. N.; Xu, Y. F.; Rao, H. S.; Su, C. Y. *Nanoscale* **2013**, *5*, 5940−5948. (d) Lana, V. T.; Boschloo, G.; Hagfeldt, A. *J. Phys. Chem. C* **2007**, *111*, 5549−5556. (e) Chen, J.; Lu, L.; Wang, W. *J. Phys. Chem. C* **2012**, *116*, 10841−10847. (f) Li, Z.; Zhou, Y.; Zhang, J.; Tu, W.; Liu, Q.; Yu, T.; Zou, Z. *Cryst. Growth Des.* **2012**, *12*, 1476−1481.

(3) (a) Shi, L.; Dai, Y. *J. Mater. Chem. A* **2013**, *1*, 12981−12986. (b) Zeng, J.; Xin, M.; Li, K.; Wang, H.; Yan, H.; Zhang, W. J. *J. Phys. Chem. C* **2008**, *112*, 4159−4167.

(4) (a) Alpuche, A. M. A.; Wu, Y. *J. Am. Chem. Soc.* **2009**, *131*, 3216−3224. (b) Zhu, H. L.; Yang, D. R.; Yu, G. X.; Zhang, H.; Jin, D. L.; Yao, K. H. *J. Phys. Chem. B* **2006**, *110*, 7631−7634.

(5) (a) Chen, H.; Wang, J.; Yu, H.; Yang, H.; Xie, S.; Li, J. *J. Phys. Chem. B* **2005**, *109*, 2573−2577. (b) Sepelak, V.; Becker, S. M.; Bergmann, I.; Indris, S.; Scheuermann, M.; Feldhoff, A.; Kubel, C.; Bruns, M.; Sturzl, N.; Ulrich, A. S.; Ghafari, M.; Hahn, H.; Grey, C. P.; Becker, K. D.; Heitjans, P. *J. Mater. Chem.* **2012**, *22*, 3117−3126. (c) Stambolova, I.; Toneva, A.; Blaskov, V.; Radev, D.; Tsvetanova, Ya; Vassilev, S.; Peshev, P. *J. Alloys Compd.* **2005**, *391*, L1−L4. (d) Fu, G.; Chen, H.; Chen, Z.; Zhang, J.; Kohler, H. *Sens. Actuators, B* **2002**, *81*, 308−312.

(6) (a) Das, P. P.; Agarkar, S. A.; Mukhopadhyay, S.; Manju, U.; Ogale, S. B.; Sujatha Devi, P. *Inorg. Chem.* **2014**, *53*, 3961−3972. (b) Banerjee, S.; Bumajdad, A.; Sujatha. Devi, P. *Nanotechnology* **2011**, *22*, 275506−275513.

(7) (a) Fan, H. J.; Yang, Y.; Zacharias, M. *J. Mater. Chem.* **2009**, *19*, 885−900. (b) Liu, B.; C. Hua, Z. *J. Am. Chem. Soc.* **2004**, *126*, 16744−16746. (c) Zolotaryov, A.; Goetze, S.; Zierold, R.; Novikov, D.; Birajdar, B.; Hesse, D.; Neilsch, K. *Adv. Eng. Mater.* **2010**, *12*, 509−516. (d) Raidongia, K.; Rao, C. N. R. *J. Phys. Chem. C* **2008**, *112*, 13366−13371.